Manipulation of molecular vibrations on condensing Er^{3+} state-densities for 1.5 μm application

Huanqing Ye*, Jelena Gorbaciova, Chen Lyu, Claire Burgess, Alex Walton, Khadisha Zahra, Richard J. Curry, Rex H.S. Bannerman, James C. Gates, Peter B. Wyatt, William P. Gillin*

Corresponding Author

Huanqing Ye - Chromosol Ltd, The Walbrook Building, 25 Walbrook, London, EC4N 8A, U.K.; Email: huanqing.ye@chromosol.com

William P. Gillin - Materials Research Institute and Department of Physics and Astronomy, Queen Mary University of London, Mile End Road, London, E1 4NS, U.K.; Chromosol Ltd, The Walbrook Building, 25 Walbrook, London, EC4N 8A, U.K.; Email: w.gillin@qmul.ac.uk

Authors

Jelena Gorbaciova, Claire Burgess - Chromosol Ltd, The Walbrook Building, 25 Walbrook, London, EC4N 8A, U.K.

Jelena Gorbaciova, Lyu Chen - Materials Research Institute and Department of Physics and Astronomy, Queen Mary University of London, Mile End Road, London, E1 4NS, U.K.

Alex S. Walton, Khadisha M. Zahra – Photon Science Institute and Department of Chemistry, FSE Research Institutes, The University of Manchester, Manchester, M13 9PL, U.K

Richard J. Curry - Photon Science Institute, Department of Electrical and Electronic Engineering, University of Manchester, Manchester M13 9PL, UK

Peter B. Wyatt - Materials Research Institute and Department of Chemistry, Queen Mary University of London, Mile End Road, London E1 4NS, U.K.

Rex H.S. Bannerman, **James C. Gates** - Zepler Institute, Faculty of Engineering and Physical Sciences, University of Southampton, Southampton, SO17 1BJ, U.K.

ABSTRACT. Vibrational modes of chemical bonds in organic erbium (Er^{3+}) materials play an important role in determining the efficiency of the 1.5 μm Er^{3+} emission. This work studies the energy coupling of the Er^{3+} intra-4f transitions and vibrational modes. The results demonstrate that the coupling introduces enormous nonradiative internal relaxation which condenses the excited erbium population on to the $^4I_{13/2}$ state. This suggests that vibrational modes can be advantageous for optimizing the branching ratio for the 1.5 μm transition in organic erbium materials. Through control of the quenching effect on to the $^4I_{13/2}$ state and a reliable determination of intrinsic radiative rates, it is found that the pump power for population inversion can be reduced by an order of magnitude at high erbium concentrations compared to conventional inorganic erbium materials.

TOC GRAPHICS

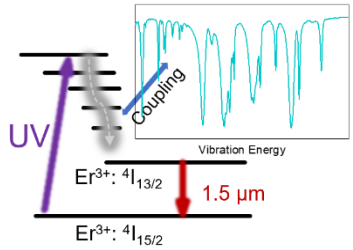

KEYWORDS

Organic Photonics; Vibrational Relaxations; Dynamic Equivalent; Population Inversion.

Silicon photonic integrated circuits (PICs) are set to pave the way for ultra-high-speed optic communications, and integrated light sources will play vital roles in producing gain regions on these PICs.[1–4] Hybrid III-V silicon integration is the current preferred approach, however there are still issues regarding their large-scale application in PICs. This inability to integrate optical gain effectively limits the complexity of PIC architectures that can be achieved. Rare-earth ion containing materials, particularly erbium (Er^{3+}), are obvious candidates as the 1.5 μm emission of Er^{3+} ions matches the low-loss telecommunication window (C-band).[5–8]. Inorganic erbium doped materials have been widely suggested but Er^{3+} solubility is commonly low and there is usually quenching at even modest ion concentrations due to energy transfer up-conversion (ETU) between clusters of ions. [9–12] Although efforts have been made to increase the solubility for higher gain capacity in a short length,[13–16] the weak absorption cross-section (10^{-21} to 10^{-20} cm^2) of Er^{3+} ions remains a drawback as high excitation power are required to reach population inversion resulting in high pump power densities on the end facet.[12,17–19]

Organic erbium materials contain organic chromophores that strongly absorb visible light to sensitize Er^{3+} excitations so as to reduce excitation power by orders of magnitude,[20–22] and approaches include polymers[23,24], single molecules[25–27] and molecular composites/hybrids. [28–31] This sensitisation means that ideally a cheap and incoherent light source (LED or integrated OLED) illuminating from the top can be used to pump organic erbium waveguides on a compact scale. In contrast to inorganic erbium materials, where the photoexcitation is into the $^4I_{13/2}$ or $^4I_{11/2}$ states, organic sensitizers usually have exciton energies > ~2 eV which will sensitize to energy states of Er^{3+} ions above the $^4I_{11/2}$ level. As some of these higher energy states are efficient visible emitters themselves, it is unknown what impact this will have on the $^4I_{13/2}$ level that is crucial for 1.5 μm emission. We study the dynamic equilibrium of excited Er^{3+} states in an organic erbium molecule by investigating the coupling of vibrational modes of the chemical bonds and the Er^{3+} intra-4f transitions. The result demonstrates that molecular

vibrations efficiently condense the excited states down to the $^4I_{13/2}$ state, which potentially reduce pump power threshold of population inversion for 1.5 μm optical gain applications. Also, we suggest a reliable approach resulting in a ~35% internal quantum efficiency (IQE) of Er^{3+} 1.5 μm emission in the organic molecule, as the highest ever.

Organic hosts usually have challenges in producing optical gain because the high vibrational energy of hydrogenated bonds (C-H, OH, or N-H) cause serious nonradiative quenching of the Er^{3+} $^4I_{13/2}$ state that limits the IQE to below 0.1%.[32,33] Fully-fluorinating organic bonds is a solution to effectively lower the vibrational energy to reduce quenching of the first excited state. Erbium (III) tetrakis(pentafluorophenyl)-imidodiphosphinate, Er(F-TPIP)$_3$[28,34] is used because the rare-earth complexes of this ligand show high thermal stability and allow for thermal deposition of thin films, which are vital for the coverage of PIC structures. The molecular structure shows a ligand cage keeping the central Er^{3+} ion at least 1.4 nm from any other Er^{3+} ion and hence reducing ion-ion interactions and the consequent ETU, although Er(F-TPIP)$_3$ has an Er^{3+} ion concentration of ~5 × 10^{20} cm^{-3}. However, its molecular nature makes it a challenge to accurately quantify the optical properties, such as the absorption cross-section for the Er^{3+} $^4I_{13/2}$ state, as large area bulk crystals are difficult to fabricate. This parameter relies on the determination of the absorption coefficient with an accurate optical path length, integration of the spectra with minimal interference from the background, refractive indices at the C-band, molecular concentrations, etc. Furthermore, hydrogenated impurities would introduce wavelength-dependent backgrounds which overlap the Er^{3+} spectral features and even distort the local ligand environment to affect the oscillator strength. Measurements on thin films are also inaccurate as, because not only the absorption coefficient of Er^{3+} $^4I_{15/2}\rightarrow{}^4I_{13/2}$ transition is too small, but also there will be strong thin-film optical interreference. Utilizing integrated spheres based on a fluorescence reference is suggested[35], however the

detection of weak Er^{3+} 1.5 μm spontaneous emission are likely to have larger uncertainties than materials that emit in the visible with larger cross-sections.

We undertake direct measurements of the Er^{3+} $^4I_{15/2}\rightarrow{}^4I_{13/2}$ absorption on a series of Er(F-TPIP)$_3$:KBr pellets varying the weight concentrations of Er(F-TPIP)$_3$. In order to subtract the background derived from the (F-TPIP$^-$)$_3$ ligand environment, we use a series of Y(F-TPIP):KBr pellets as reference backgrounds that contain similar weight concentrations of Er(F-TPIP)$_3$, where Y^{3+} refers to optically inert yttrium (III) ions. To minimise the effect of KBr powder on the Er^{3+} spectral feature, Er(F-TPIP)$_3$ weight concentrations are employed with 75wt%, 94wt% and 100wt% to have the Er^{3+} signals clearly stronger than scattered backgrounds. An average absorption cross-section spectrum is shown in **Figure 1a**. The integral of the absorption cross-section spectrum ($\sigma[^4I_{15/2}\rightarrow{}^4I_{13/2}]$) shows a linear response to the Er(F-TPIP)$_3$ concentrations. The refractive index at 1.55 μm of Er(F-TPIP)$_3$ was measured using a Prism coupler on 3 μm thin-films thermally evaporated on to a silicon wafer. Fitting the data [See Supplementary information (SI)] gives a radiative rate ($k_{rad}[^4I_{13/2}\rightarrow{}^4I_{15/2}]$) of 354 ± 12 s^{-1} for the Er^{3+} $^4I_{13/2}\rightarrow{}^4I_{15/2}$ transition. This number is larger than that reported on a micro-size crystal of Er(F-TPIP)$_3$ precipitated from a DMSO solution.[36] The inaccuracy for crystal samples can be attributed to uncertainties in determining the refractive indices, the measured thickness, the full spectral width and the effect on the spectral background due to hydrogenated impurities.

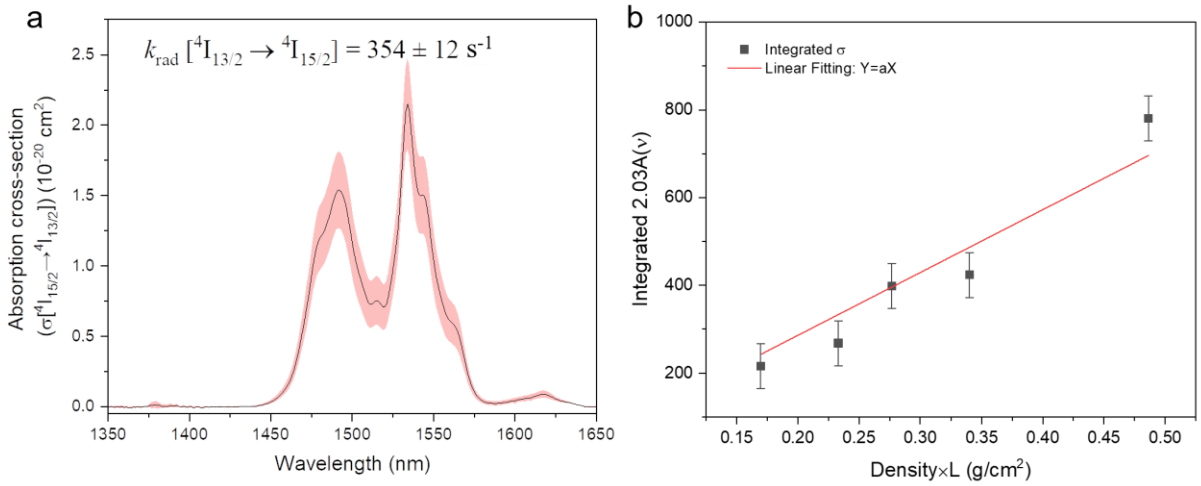

Figure 1. (a) The spectrum of the average absorption cross-section of $Er(F\text{-}TPIP)_3$ in KBr pellets. Error bars on the Y-axis are colour filled. (b) Fitting the integral of the absorbance spectra against various $Er(F\text{-}TPIP)_3$ densities multiplied by the optical path.

Once the intrinsic radiative rate is known, one only needs to measure the 1.5 μm emission lifetime to determine the IQE of the $^4I_{15/2} \rightarrow {}^4I_{13/2}$ transition. As was reported for $Yb(F\text{-}TPIP)_3$,[37] it is vital to keep water vapour in the air from diffusing into the material in order to obtain the natural radiative lifetime. Hence, we fabricate thin films in a thermal evaporation system pumped by a cryopump to an ultra-high-vacuum (UHV) condition. Under such conditions, we minimise the chance of water molecules being trapped in the films during growth. The thin films are deposited on to polished silica substrates and a 500 nm thick aluminium layer is deposited after as an encapsulation. The encapsulated film sample gives a 1.5 μm PL lifetime of 0.97±0.1 ms using direct excitation into the Er^{3+} $^2H_{11/2}$ level. Diluting $Er(F\text{-}TPIP)_3$ to 20% in a $Er_{0.2}Y_{0.8}(F\text{-}TPIP)_3$ composite film (with encapsulation) gives a PL lifetime of 1.04±0.10 ms (**Figure 2a**). This can be attributed to the fact that the shell of the $(F\text{-}TPIP^-)_3$ ligands, keeping any two Er^{3+} ions separated by at least 1.4 nm, prevents the Er^{3+}-Er^{3+} ion pairs from concentration quenching, which is a common problem that limit the performance of erbium containing glasses. These result shows that we could optimize the IQE for 1.5 μm PL to be

~35% with good control of fabrication conditions. Without encapsulation the PL lifetime is dramatically quenched and has two components with lifetimes of 0.31±0.07 ms (75% component) and 0.65±0.02 ms (25% component). Long term exposure of an unencapsulated film to air results in the lifetime becoming single exponential with a lifetime of ~200 μs. As this lifetime can be increased if the sample is measured in vacuum, and return to this value when exposed to air, we believe that the in-diffusion of water molecules into the film is the most likely cause. Assuming Förster energy transfer between the excited $^4I_{13/2}$ level and a random distribution of water molecules in the film we were able to estimate a maximal water concentration in the film of ~8×10^{20} cm^{-3} (in the SI) and a Förster radius of ~0.97 nm. These values have a very large uncertainty (and are almost certainly an overestimate) due to the approximations used. But, with a Förster radius larger than the radius of an $Er(F\text{-}TPIP)_3$ molecule (~0.7 nm) it implies that there is less than, but of the order of, one water molecule present in the film for every $Er(F\text{-}TPIP)_3$ molecule. We have used x-ray photoelectron spectroscopy (XPS) in the SI to look at the O 1s peak in similar films of $Er(F\text{-}TPIP)_3$. These results show that there are two environments for the oxygen. The major peak corresponds to the P=O bonds in the $Er(F\text{-}TPIP)_3$ molecule, whilst a high energy shoulder is consistent with the binding energy for water. Taking the ratio of these two peaks we can obtain a water concentration that is about 25% of the Er^{3+} concentration. Given that we have seen that water appears to diffuse from the films on exposure to vacuum these results are comparable to the Förster calculations and imply that without encapsulation a significant amount of water is present in the films and is responsible for quenching.

To investigate the internal relaxations within these states we use a 377 nm laser to directly excite the $^2G_{9/2}$ state and the Er^{3+} PL spectrum is shown in **Figure 2b**. The calculated branching ratios for relaxations from the $^4G_{11/2}$ to the lower states were calculated from a Judd-Ofelt (JO) analysis and are listed in **Table S2**.[36,38–40] **Figure 2b** also shows the calculated theoretical

emission intensities of the $^2H_{11/2}$, $^4F_{9/2,}$ $^4I_{9/2}$ and $^4I_{11/2}$ states, from the JO analysis and are the emissions expected with no internal quenching, normalized to the $^4I_{13/2}$ emission intensity. The emission from the $^2H_{11/2}$, $^4F_{9/2,}$ $^4I_{9/2}$ have all disappeared (even when the scale is multiplied by a factor of 100), whilst the emission from the $^4I_{11/2}$ level is <0.5% of that expected when compared to the intensity of the $^4I_{13/2}$ emission.

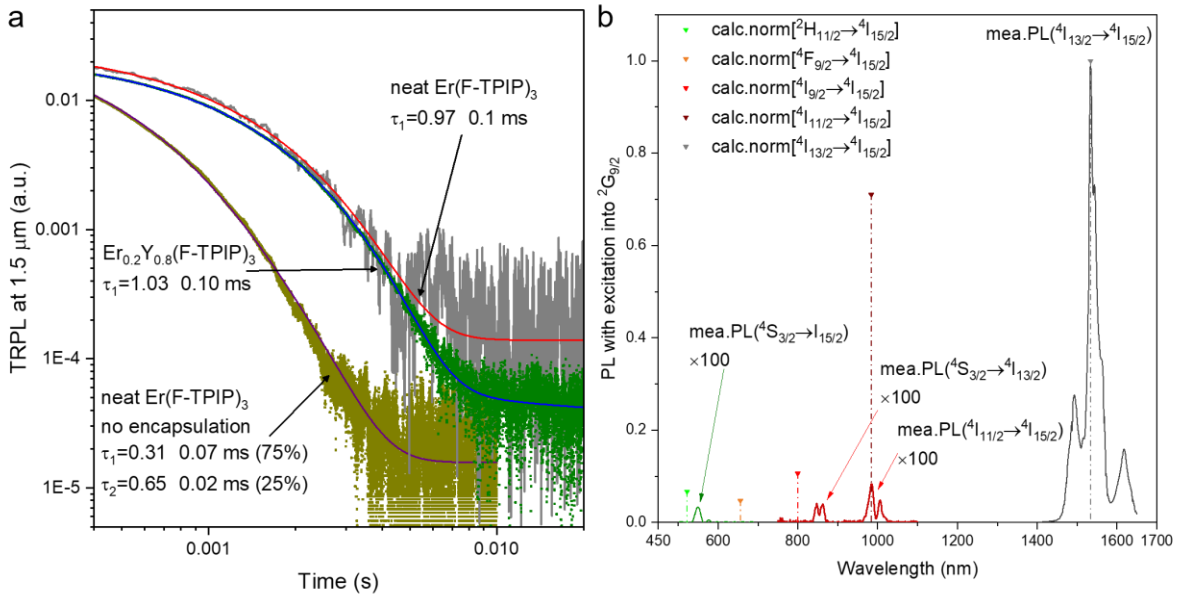

Figure 2. (a) Comparisons of TRPL spectra of Er(F-TPIP)$_3$ thin films with dilution, encapsulations, and no encapsulations. (b) The experimental Er(F-TPIP)$_3$ PL spectrum with excitation into $^2G_{9/2}$. The PL spectra below 1200 nm is magnified by 100 times. The theoretical normalised intensities of the transitions are indicated as coloured triangles with drop lines. Note that these are on the original scale and hence the PL is >100 times weaker than expected.

We attribute this difference in the emission intensities to strong coupling with vibrations of the chemical bonds in the molecule. The FTIR spectrum of Er(F-TPIP)$_3$ powder shows vibrational features at wavenumbers below 1000 cm^{-1} and **Figure 3** shows that the fundamental, 1st and 2nd overtones of the vibrational spectra overlap the energy gap of several of the internal transitions such as $^2H_{11/2}\rightarrow{}^4S_{3/2,}$ $^2H_{11/2}\rightarrow{}^4F_{9/2}$, $^4F_{9/2}\rightarrow{}^4I_{9/2}$, $^2I_{9/2}\rightarrow{}^4I_{11/2}$ and $^2I_{11/2}\rightarrow{}^4I_{13/2}$. This overlap suggests that nonradiative or thermal relaxations should be inevitable and hence we

have used a Förster analysis to quantify them. **Figure 3a** shows the simulated molar absorption coefficients of the overtone vibrations. The peak absorption cross-section of the C=C stretch is between ~5 × 10^{-20} to ~1 × 10^{-19} cm^2.[41–43] Hence, we can evaluate the peak absorption cross-section of C=C stretch at 1476 cm^{-1} as within the range,[41,44] and convert the number to the molar absorption coefficient on the FTIR spectrum of the fundamental overtone. Furthermore, we simulate the molar absorption coefficients of the 1st to 2nd overtone spectra, using reported empirical results that suggest the amplitude of overtone vibrations will decrease by an order of the magnitude. [44]

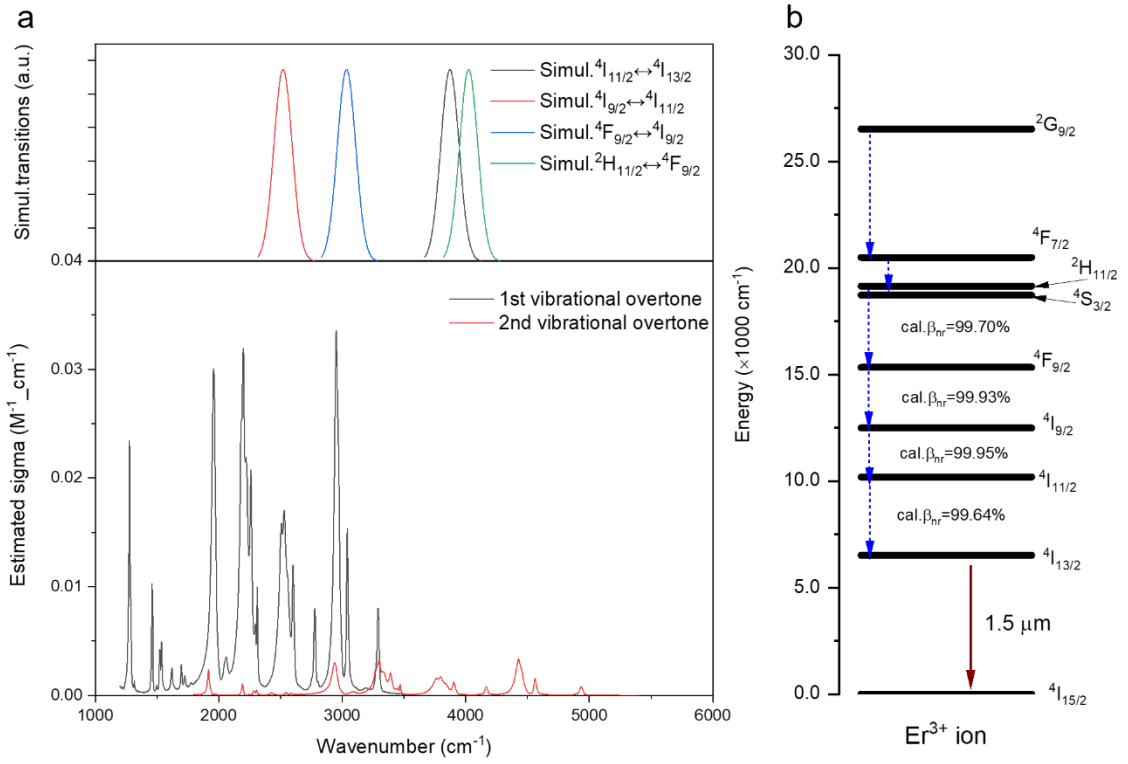

Figure 3. (a) The overlap of the vibrational and overtone (1st, 2nd) spectra and the simulated normalized spectra of the $^4I_{11/2}\leftrightarrow{}^4I_{13/2}$, $^4I_{9/2}\leftrightarrow{}^4I_{11/2}$, $^4F_{9/2}\leftrightarrow{}^4I_{9/2}$ and $^2H_{11/2}\leftrightarrow{}^4F_{9/2}$ transitions. (b) Calculated branching ratios for nonradiative transitions. The dashed arrows indicate the nonradiative relaxation.

According to the reported crystallographic data of $Er(F\text{-}TPIP)_3$[34], the molecular radius is ~ 0.7 nm and it suggests an effective Förster radius between vibrational bonds on the ligand and the Er^{3+} ions would be at most this radius. Therefore, using 0.7 nm as a Förster radius we can calculate the nonradiative rates for the $^2H_{11/2}\rightarrow{}^4S_{3/2}$, $^2H_{11/2}\rightarrow{}^4F_{9/2}$, $^4F_{9/2}\rightarrow{}^4I_{9/2}$, $^2I_{9/2}\rightarrow{}^4I_{11/2}$ and $^2I_{11/2}\rightarrow{}^4I_{13/2}$ transitions. The results, when compared to the corresponding radiative transition rates, show that the non-radiative rates are orders of magnitude larger, as listed in **Table S2**. Noteworthily, the actual Förster radius might be significantly smaller than the molecular radius so that those nonradiative transition rates could be even higher than the simulated results. These simulated values mean the population at these excited states will rapidly undergo nonradiative transitions to the $^4I_{13/2}$ state with the branching ratios (β_{nr}) for these non-radiative relaxations of > 99%. This performance shows a clear difference compared to inorganic erbium materials such as Er^{3+}-doped nanoparticles, where green ~ 522 nm ($^2H_{11/2}\rightarrow{}^4F_{9/2}$), red ~ 655 nm ($^4F_{9/2}\rightarrow{}^4I_{9/2}$) and NIR ~980 nm ($^2I_{9/2}\rightarrow{}^4I_{11/2}$) emission are particularly bright. Particularly, the intrinsic high branching ratio for hypersensitive $^2H_{11/2}\rightarrow{}^4I_{15/2}$ is replaced by a rapid relaxation to $^4S_{3/2}$ followed by a 99.7% non-radiative relaxation towards $^4F_{9/2}$. It is interesting that we can still observe weak PL at ~ 534 nm and ~850 nm and their energies match the $^4S_{3/2}\rightarrow{}^4I_{15/2}$ and $^4S_{3/2}\rightarrow{}^4I_{13/2}$ transitions, respectively. Due to the strong interaction between the $^2H_{11/2}\rightarrow{}^4S_{3/2}$ transition and the molecular absorption there is complete relaxation to the $^4S_{3/2}$ level. The $^4S_{3/2}\rightarrow{}^4F_{9/2}$ transition is "only" 99.7% quenched and hence there is some population on the $^4S_{3/2}$ which allows the $^4S_{3/2}\rightarrow{}^4I_{15/2}$ and $^4S_{3/2}\rightarrow{}^4I_{13/2}$ transitions to be experimentally observed with low intensity.

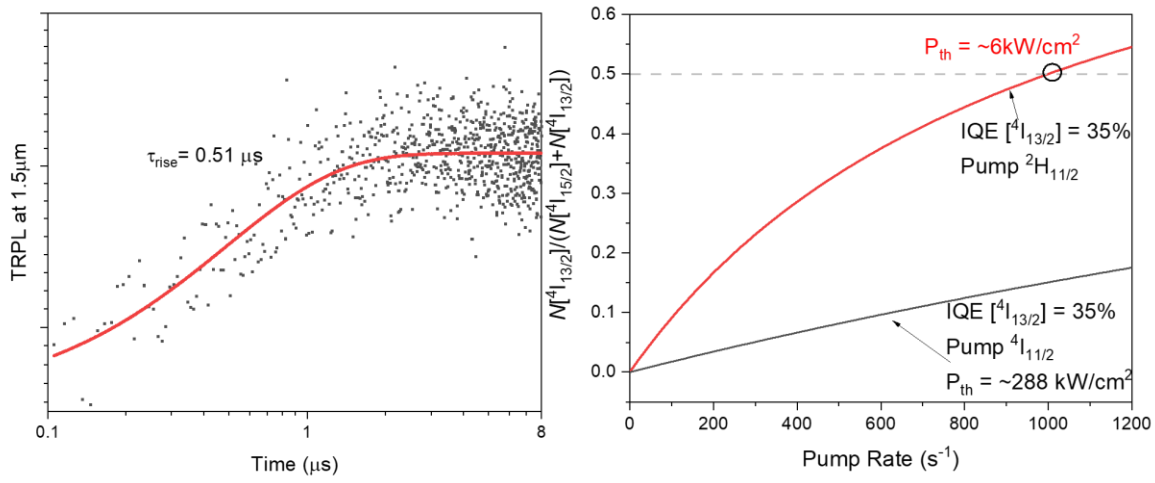

Figure 4. (a) TRPL rise time of an encapsulated Er(F-TPIP)$_3$ thin film with photoexcitation into $^2H_{11/2}$ with a 5ns pulsed 522 nm laser. (b) Comparison of the modelling $N[^4I_{13/2}]/ N[^4I_{15/2}]$ with the nonradiative internal relaxation rates (k_{nr}) at the photoexcitation into $^4I_{11/2}$ and $^2H_{11/2}$.

The nonradiative internal relaxations allow us to concentrate excited Er^{3+} ions onto the $^4I_{13/2}$ state faster than allowed from the intrinsic transitions. **Figure 4a** gives the measured rise time for the $^4I_{13/2}$ state ~ 0.5 µs, compared to a calculated rise time of ~ 6 ms (see the SI) for excitation into the $^2H_{11/2}$ state. This rapid condensing will dramatically reduce the pump power required to obtain population inversion, as shown in **Figure 4b**, we plot the ratio of the calculated population of the $^4I_{13/2}$ and $^4I_{15/2}$ states, under excitation into the $^2H_{11/2}$ level, where a value of 0.5 means that population inversion has been achieved. Assuming an IQE of 35% we can achieve population inversion at a threshold of ~ 6kW/cm^2 compared to ~100kW/cm^2 which is common for inorganic erbium doped gain media (when pumped into the $^4I_{11/2}$ level). However, using an organic chromophore as a sensitizer allows for an ~10,000 times increase in the effective cross-section and implies that this power density can be decreased to <1W/cm^2.[45] Another advantage is that it is possible to eliminate losses due to ETU which are likely excited-state-absorption (ESA) processes with $^4I_{11/2}$-$^4I_{11/2}$ or $^4I_{11/2}$-$^4I_{13/2}$ interactions and

cooperative up-conversion (CUC) with $^4I_{13/2}$-$^4I_{13/2}$ interactions. In Er(F-TPIP)$_3$, the overtone vibrations will quench the $^4I_{11/2}$ state and hence reduce ESA processes and will relax CUC-induced $^4I_{11/2}$ excitations to the $^4I_{13/2}$ state instead of the ground $^4I_{15/2}$ state, meaning that only one excitation is lost instead of two. However, as mentioned for **Figure 2** the F-TPIP$^-$ shell separates any two ions by 1.4 nm and hence the probability for interactions is reduced compared to inorganic hosts where clustering can occur even at lower ion concentrations.

Conclusions

The diffusion of water molecules from the ambient environment is a sever problem that reduces the IQE of Er^{3+} 1.5 μm emission for organic erbium molecular materials, hence an encapsulation is employed and has optimized the IQE to ~ 35%. Meanwhile, molecular vibrations play a vital role in condensing excited Er^{3+} ions to its $^4I_{13/2}$ level. Our numerical simulation suggests this condensation will reduce pump power significantly for the population inversion and eliminate possible ETU processes. The results suggest the organic erbium material could be a competing alternative to conventionally utilized inorganic erbium materials regarding the development of cost-effective 1.5 μm optical gain media on PICs.

Experimental Methods

The organic complex Er(F-TPIP)$_3$ is synthesised according to the published methods. The chemical products of HFTPIP were supplied by Chromosol Ltd. $ErCl_3 \cdot 6H_2O$ was purchased from Alfa Aesar. The crude material is purified by using a train vacuum purification system. Organic thin films were fabricated in a Chi-Vac UHV thermal evaporation system. The photoluminescence signals are collected by a Horiba Triax 550 spectrometer and detected using a Hamamatsu R5509-72 nitrogen-cooled photomultiplier.

Supporting Information

Details of absorption measurements, calculation of branching ratios, Förster calculation and rate equation simulation are included in the supporting information.

Competing interests

WPG is the founder of Chromosol Ltd which uses these materials to build erbium-based gain regions on to phonic integrated circuits. JG and HQY are employees of Chromosol. PBW is a shareholder in Chromosol.

Acknowledgment

CL was financially supported by the China Scholarship Council and Queen Mary University of London. WPG acknowledges financial support from IUK (79053) and EPSRC (EP/L020114/1 and EP/P007767/1). XPS measurements in this work were performed at the Henry Royce Institute for Advanced Materials, funded through EPSRC grants EP/R00661X/1 and EP/P025021/1.

Reference:

(1) Fang, Z.; Chen, Q. Y.; Zhao, C. Z. A Review of Recent Progress in Lasers on Silicon. *Optics and Laser Technology*. March 2013, pp 103–110.

(2) Kelsall, R. W. Rubber Stamp for Silicon Photonics. *Nat. Photonics* **2012**, *6* (September), 577–579.

(3) Soref, R. The Past, Present, and Future of Silicon Photonics. *IEEE J. Sel. Top. Quantum Electron.* **2006**, *12* (6), 1678–1687.

(4) Stampoulidis, L.; Vyrsokinos, K.; Voigt, K.; Zimmermann, L.; Gomez-Agis, F.; Dorren, H. J. S.; Sheng, Z.; Van Thourhout, D.; Moerl, L.; Kreissl, J.; et al. The European BOOM Project: Silicon Photonics for High-Capacity Optical Packet Routers. *IEEE J. Sel. Top. Quantum Electron.* **2010**, *16* (5), 1422–1433.

(5) Frolov, S.; Shen, T.-M.; Bruce, A. J. EDWA: Key Enabler of Optical Integration on

PLC. In *Rare-Earth-Doped Materials and Devices VII*; SPIE, 2003; Vol. 4990, p 47.

(6) Pollnau, M. Rare-Earth-Ion-Doped Waveguide Lasers on a Silicon Chip. In *Optical Components and Materials XII*; SPIE, 2015; Vol. 9359, p 935910.

(7) Bradley, J. D. B.; Hosseini, E. S.; Purnawirman; Su, Z.; Adam, T. N.; Leake, G.; Coolbaugh, D.; Watts, M. R. Monolithic Erbium- and Ytterbium-Doped Microring Lasers on Silicon Chips. *Opt. Express* **2014**, *22* (10), 12226.

(8) Patel, F. D.; DiCarolis, S.; Lum, P.; Venkatesh, S.; Miller, J. N. A Compact High-Performance Optical Waveguide Amplifier. *IEEE Photonics Technol. Lett.* **2004**, *16* (12), 2607–2609.

(9) Agazzi, L.; Bradley, J. D. B.; Dijkstra, M.; Ay, F.; Roelkens, G.; Baets, R.; Wörhoff, K.; Pollnau, M. Monolithic Integration of Erbium-Doped Amplifiers with Silicon-on-Insulator Waveguides. *Opt. Express* **2010**, *18* (26), 27703.

(10) Bradley, J. D. B.; Pollnau, M. Erbium-Doped Integrated Waveguide Amplifiers and Lasers. *Laser Photon. Rev.* **2011**, *5* (3), 368–403.

(11) Kik, P. G.; Polman, A. Erbium-Doped Optical-Waveguide Amplifiers on Silicon. *MRS Bull.* **1998**, *23* (4), 48–54.

(12) Sun, H.; Yin, L.; Liu, Z.; Zheng, Y.; Fan, F.; Zhao, S.; Feng, X.; Li, Y.; Ning, C. Z. Giant Optical Gain in a Single-Crystal Erbium Chloride Silicate Nanowire. *Nat. Photonics* **2017**, *11* (9), 589–593.

(13) Agazzi, L.; Wörhoff, K.; Pollnau, M. Energy-Transfer-Upconversion Models, Their Applicability and Breakdown in the Presence of Spectroscopically Distinct Ion Classes: A Case Study in Amorphous Al2O3:Er3+. *J. Phys. Chem. C* **2013**, *117* (13),

6759–6776.

(14) Pollnau, M.; Jackson, S. D. Energy Recycling versus Lifetime Quenching in Erbium-Doped 3-Mm Fiber Lasers. *IEEE J. Quantum Electron.* **2002**, *38* (2), 162–169.

(15) Vázquez-Córdova, S. A.; Dijkstra, M.; Bernhardi, E. H.; Ay, F.; Wörhoff, K.; Herek, J. L.; García-Blanco, S. M.; Pollnau, M. Erbium-Doped Spiral Amplifiers with 20 DB of Net Gain on Silicon. *Opt. Express* **2014**, *22* (21), 25993.

(16) Kik, P. G.; Polman, A. Cooperative Upconversion as the Gain-Limiting Factor in Er Doped Miniature Al2O3 Optical Waveguide Amplifiers. *J. Appl. Phys.* **2003**, *93* (9), 5008–5012.

(17) Frankis, H. C.; Mbonde, H. M.; Bonneville, D. B.; Zhang, C.; Mateman, R.; Leinse, A.; Bradley, J. D. B. Erbium-Doped TeO 2 -Coated Si 3 N 4 Waveguide Amplifiers with 5 DB Net Gain . *Photonics Res.* **2020**, *8* (2), 127.

(18) Belt, M.; Blumenthal, D. J. Erbium-Doped Waveguide DBR and DFB Laser Arrays Integrated within an Ultra-Low-Loss Si_3N_4 Platform. *Opt. Express* **2014**, *22* (9), 10655.

(19) Purnawirman; Sun, J.; Adam, T. N.; Leake, G.; Coolbaugh, D.; Bradley, J. D. B.; Hosseini, E. S.; Watts, M. R. C- and L-Band Erbium-Doped Waveguide Lasers with Wafer-Scale Silicon Nitride Cavities. *Opt. Lett.* **2013**, *38* (11), 1760.

(20) Hernández, I.; Gillin, W. P. Organic Chromophores-Based Sensitization of NIR-Emitting Lanthanides: Toward Highly Efficient Halogenated Environments. In *Handbook on the Physics and Chemistry of Rare Earths*; Elsevier, 2015; Vol. 47, pp 1–100.

(21) Bünzli, J.-C. G. On the Design of Highly Luminescent Lanthanide Complexes. *Coord. Chem. Rev.* **2015**, *293–294*, 19–47.

(22) Zou, W.; Visser, C.; Maduro, J. A.; Pshenichnikov, M. S.; Hummelen, J. C. Broadband Dye-Sensitized Upconversion of near-Infrared Light. *Nat. Photonics* **2012**, *6* (8), 560–564.

(23) Wang, T.; Zhao, D.; Zhang, M.; Yin, J.; Song, W.; Jia, Z.; Wang, X.; Qin, G.; Qin, W.; Wang, F.; et al. Optical Waveguide Amplifiers Based on NaYF_4: Er^3+, Yb^3+ NPs-PMMA Covalent-Linking Nanocomposites. *Opt. Mater. Express* **2015**, *5* (3), 469.

(24) Ashoka Sahadevan, S.; Monni, N.; Abhervé, A.; Marongiu, D.; Sarritzu, V.; Sestu, N.; Saba, M.; Mura, A.; Bongiovanni, G.; Cannas, C.; et al. Nanosheets of Two-Dimensional Neutral Coordination Polymers Based on Near-Infrared-Emitting Lanthanides and a Chlorocyananilate Ligand. *Chem. Mater.* **2018**, *30* (18), 6575–6586.

(25) Chen, P.-Z.; Zhang, H.; Niu, L.-Y.; Zhang, Y.; Chen, Y.-Z.; Fu, H.-B.; Yang, Q.-Z. A Solid-State Fluorescent Material Based on Carbazole-Containing Difluoroboron β-Diketonate: Multiple Chromisms, the Self-Assembly Behavior, and Optical Waveguides. *Adv. Funct. Mater.* **2017**, *27* (25), 1700332.

(26) Davis, D.; Carrod, A. J.; Guo, Z.; Kariuki, B. M.; Zhang, Y. Z.; Pikramenou, Z. Imidodiphosphonate Ligands for Enhanced Sensitization and Shielding of Visible and Near-Infrared Lanthanides. *Inorg. Chem.* **2019**, *58* (19), 13268–13275.

(27) Martín-Ramos, P.; Martín, I. R.; Lahoz, F.; Hernández-Navarro, S.; Pereira Da Silva, P. S.; Hernández-Campo, I.; Lavín, V.; Ramos Silva, M. An Erbium(III)-Based NIR Emitter with a Highly Conjugated β-Diketonate for Blue-Region Sensitization. *J. Alloys Compd.* **2015**, *619*, 553–559.

(28) Ye, H. Q.; Li, Z.; Peng, Y.; Wang, C. C.; Li, T. Y.; Zheng, Y. X.; Sapelkin, A.; Adamopoulos, G.; Hernández, I.; Wyatt, P. B.; et al. Organo-Erbium Systems for Optical Amplification at Telecommunications Wavelengths. *Nat. Mater.* **2014**, *13* (4), 382–386.

(29) Binnemans, K. Lanthanide-Based Luminescent Hybrid Materials | Koen Binnemans - Academia.Edu. *Chem. Rev.* **2009**, *109*, 4283–4374.

(30) Li, H. F.; Liu, X. Q.; Lyu, C.; Gorbaciova, J.; Wen, L. L.; Shan, G. G.; Wyatt, P. B.; Ye, H. Q.; Gillin, W. P. Enhanced 1.54-Mm Photo- and Electroluminescence Based on a Perfluorinated Er(III) Complex Utilizing an Iridium(III) Complex as a Sensitizer. *Light Sci. Appl.* **2020**, *9* (1), 1–10.

(31) Zhang, D.; Li, W.; Chu, B.; Li, X.; Han, L.; Zhu, J.; Li, T.; Bi, D.; Yang, D.; Yan, F.; et al. Sensitized Photo- and Electroluminescence from Er Complexes Mixed with Ir Complex. *Appl. Phys. Lett.* **2008**, *92* (9), 093501.

(32) Winkless, L.; Tan, R. H. C. C.; Zheng, Y.; Motevalli, M.; Wyatt, P. B.; Gillin, W. P. Quenching of Er (III) Luminescence by Ligand CH Vibrations: Implications for the Use of Erbium Complexes in Telecommunications. *Appl. Phys. Lett.* **2006**, *89* (11), 1115.

(33) Doffek, C.; Alzakhem, N.; Bischof, C.; Wahsner, J.; Güden-Silber, T.; Lügger, J.; Platas-Iglesias, C.; Seitz, M. Understanding the Quenching Effects of Aromatic C-H- and C-D-Oscillators in near-IR Lanthanoid Luminescence. *J. Am. Chem. Soc.* **2012**, *134* (39), 16413–16423.

(34) Glover, P. B.; Bassett, A. P.; Nockemann, P.; Kariuki, B. M.; Van Deun, R.; Pikramenou, Z. Fully Fluorinated Imidodiphosphinate Shells for Visible- and NIR-

Emitting Lanthanides: Hitherto Unexpected Effects of Sensitizer Fluorination on Lanthanide Emission Properties. *Chem. - A Eur. J.* **2007**, *13* (22), 6308–6320.

(35) Shavaleev, N. M.; Scopelliti, R.; Gumy, F.; Bünzli, J. C. G. Surprisingly Bright Near-Infrared Luminescence and Short Radiative Lifetimes of Ytterbium in Hetero-Binuclear Yb-Na Chelates. *Inorg. Chem.* **2009**, *48* (16), 7937–7946.

(36) Ye, H. Q.; Peng, Y.; Li, Z.; Wang, C. C.; Zheng, Y. X.; Motevalli, M.; Wyatt, P. B.; Gillin, W. P.; Hernández, I. Effect of Fluorination on the Radiative Properties of Er3+ Organic Complexes: An Opto-Structural Correlation Study. *J. Phys. Chem. C* **2013**, *117* (45), 23970–23975.

(37) Ye, H.; Bogdanov, V.; Liu, S.; Vajandar, S.; Osipowicz, T.; Hernández, I.; Xiong, Q. Bright Photon Upconversion on Composite Organic Lanthanide Molecules through Localized Thermal Radiation. *J. Phys. Chem. Lett.* **2017**, *8* (23), 5695–5699.

(38) Sardar, D. K.; Gruber, J. B.; Zandi, B.; Hutchinson, J. A.; Ward Trussell, C. Judd-Ofelt Analysis of the Er3+(4f11) Absorption Intensities in Phosphate Glass: Er3+, Yb3+. *J. Appl. Phys.* **2003**, *93* (4), 2041–2046.

(39) Li, A.; Sun, L.; Zheng, Z.; Wu, W.; Liu, W.; Yang, Y.; Lü, T.; Su, W. Spectroscopic Analysis of Er3+ Transition in Mg/Er-Codoped LiNbO3 Crystal. *J. Lumin.* **2008**, *128* (2), 239–244.

(40) Desirena, H.; De La Rosa, E.; Díaz-Torres, L. A.; Kumar, G. A. Concentration Effect of Er3+ Ion on the Spectroscopic Properties of Er3+ and Yb3+/Er3+ Co-Doped Phosphate Glasses. *Opt. Mater. (Amst).* **2006**, *28* (5), 560–568.

(41) Reddy, K. V.; Heller, D. F.; Berry, M. J. Highly Vibrationally Excited Benzene:

Overtone Spectroscopy and Intramolecular Dynamics of C6H6, C6D 6, and Partially Deuterated or Substituted Benzenes. *J. Chem. Phys.* **1982**, *76* (6), 2814–2837.

(42) Koszykowski, M. L.; Nold, D. W.; Marcus, R. A. Semiclassical Theory of Intensities of Vibrational Fundamentals, Overtones, and Combination Bands; *J. Phys. Chem.* **1982**; *86* (12), 2113-2117.

(43) Etzkorn, T.; Klotz, B.; Sørensen, S.; Patroescu, I. V.; Barnes, I.; Becker, K. H.; Platt, U. Gas-Phase Absorption Cross Sections of 24 Monocyclic Aromatic Hydrocarbons in the UV and IR Spectral Ranges. *Atmos. Environ.* **1999**, *33* (4), 525–540.

(44) Phillips, J. A.; Orlando, J. J.; Tyndall, G. S.; Vaida, V. Integrated Intensities of OH Vibrational Overtones in Alcohols. *Chem. Phys. Lett.* **1998**, *296* (3–4), 377–383.

(45) Hu, J. X.; Karamshuk, S.; Gorbaciova, J.; Ye, H. Q.; Lu, H.; Zhang, Y. P.; Zheng, Y. X.; Liang, X.; Hernández, I.; Wyatt, P. B.; et al. High Sensitization Efficiency and Energy Transfer Routes for Population Inversion at Low Pump Intensity in Er Organic Complexes for IR Amplification. *Sci. Rep.* **2018**, *8* (1), 3226.